JACS
JOURNAL OF THE AMERICAN CHEMICAL SOCIETY
Article
pubs.acs.org/JACS

Controlled Conjugated Backbone Twisting for an Increased Open-Circuit Voltage while Having a High Short-Circuit Current in Poly(hexylthiophene) Derivatives

Sangwon Ko,[†] Eric T. Hoke,[‡] Laxman Pandey,[§] Sanghyun Hong,[⊥] Rajib Mondal,[⊥] Chad Risko,[§] Yuanping Yi,[§] Rodrigo Noriega,[‡] Michael D. McGehee,[∥] Jean-Luc Brédas,[§] Alberto Salleo,[∥] and Zhenan Bao*,[⊥]

[†]Department of Chemistry, [‡]Department of Applied Physics, [⊥]Department of Chemical Engineering, and [∥]Department of Materials Science and Engineering, Stanford University, Stanford, California 94305, United States

[§]School of Chemistry and Biochemistry, Georgia Institute of Technology, Atlanta, Georgia 30332, United States

Supporting Information

ABSTRACT: Conjugated polymers with nearly planar backbones have been the most commonly investigated materials for organic-based electronic devices. More twisted polymer backbones have been shown to achieve larger open-circuit voltages in solar cells, though with decreased short-circuit current densities. We systematically impose twists within a family of poly(hexylthiophene)s and examine their influence on the performance of polymer:fullerene bulk heterojunction (BHJ) solar cells. A simple chemical modification concerning the number and placement of alkyl side chains along the conjugated backbone is used to control the degree of backbone twisting. Density functional theory calculations were carried out on a series of oligothiophene structures to provide insights on how the sterically induced twisting influences the geometric, electronic, and optical properties. Grazing incidence X-ray scattering measurements were performed to investigate how the thin-film packing structure was affected. The open-circuit voltage and charge-transfer state energy of the polymer:fullerene BHJ solar cells increased substantially with the degree of twist induced within the conjugated backbone—due to an increase in the polymer ionization potential—while the short-circuit current decreased as a result of a larger optical gap and lower hole mobility. A controlled, moderate degree of twist along the poly(3,4-dihexyl-2,2′:5′,2″-terthiophene) (PDHTT) conjugated backbone led to a 19% enhancement in the open-circuit voltage (0.735 V) vs poly(3-hexylthiophene)-based devices, while similar short-circuit current densities, fill factors, and hole-carrier mobilities were maintained. These factors resulted in a power conversion efficiency of 4.2% for a PDHTT:[6,6]-phenyl-C_{71}-butyric acid methyl ester ($PC_{71}BM$) blend solar cell without thermal annealing. This simple approach reveals a molecular design avenue to increase open-circuit voltage while retaining the short-circuit current.

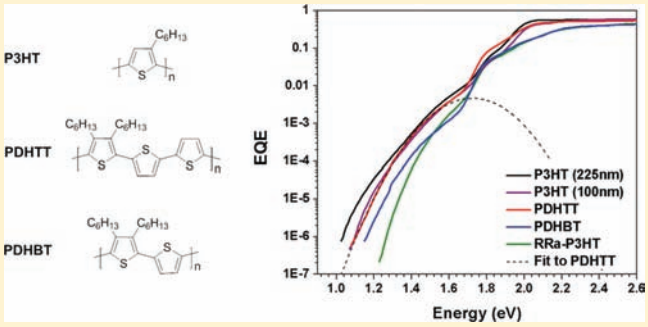

INTRODUCTION

The performance of bulk heterojunction (BHJ) solar cells has steadily improved over the past few years, with power conversion efficiencies (PCEs) recently pushing over 8% for polymer:fullerene blends.[1] Much of the improvement can be attributed to the design of new polymers with (i) increased ionization potentials (IPs) to achieve large open-circuit voltages (V_{oc}) and (ii) reduced optical gaps to increase the short-circuit current (J_{sc}). The optimization of functional polymers has primarily focused on the engineering of the conjugated backbone.[2−5] By controlling the number[4] and the strength of the electron-donating or electron-withdrawing substituents,[6,7] one can readily modify both the polymer IP and, hence, the device V_{oc}. The side chains can also impact the polymer electronic properties. Conjugated side chains have been incorporated to increase the extent of conjugated regions so as to broaden light absorption;[8,9] the substituent investigated in these studies, however, produce devices with limited PCEs and low J_{sc}, possibly due to a smaller charge-carrier mobility (caused by excessive twisting in the polymer backbone) or reduced absorption coefficients (due to a reduction in the spatial overlap of the highest occupied molecular orbital (HOMO) and lowest unoccupied molecular orbital (LUMO) wave functions).[10]

Structural modification to the geometry of the conjugated backbone provides an additional route to influence the electronic and optical properties. The degree of curvature within the conjugated backbone has been shown to have considerable impact on the polymer electronic properties, film morphology, and charge-carrier mobility.[11] The curvature (or zigzag pattern) of poly(thienothiophene−benzodithiophene) systems has been suggested as a distinct feature leading to face-

Received: November 21, 2011
Published: March 2, 2012

   dx.doi.org/10.1021/ja210954r | J. Am. Chem. Soc. 2012, 134, 5222−5232

on π-stacking with respect to the substrate and improved charge-transport across the interface.[12] Sterically induced twisting of the polymer backbone has been shown to influence the energy levels of conjugated polymers through modification of the conjugation length along the backbone. Andersson and co-workers showed that the optical gap of polythiophenes can be tuned by nearly 1 eV by varying the side-chain bulkiness.[13] Bulky substituents increase the degree of twisting (from planarity) in the backbone, resulting in a decreased conjugation length and larger optical gaps vs less bulky/linear substituents. While it is often assumed that bulky substituents hinder charge transport and thus are detrimental for organic solar cells, they have been shown to increase V_{oc} in small-molecule bilayer solar cells, which was attributed to a reduction the intermolecular interactions between the donor and acceptor materials at the interface, resulting in a smaller dark current.[14] A similar investigation of the influence of side-chain-induced polymer backbone twisting on the performance of polymer:fullerene solar cells has yet to be performed.

Polythiophene derivatives are attractive systems for investigating the influence of backbone twisting due to their facile preparation with various substituents. Recently we demonstrated that 3,4-disubstituted polyalkylthiophenes, which do not show distinct $\pi-\pi$ stacking, can be used to make thin-film transistors (TFTs) and BHJ solar cells that rival benchmark poly(3-hexylthiophene) (P3HT) devices.[15] Herein, we present a systematic study of how sterically induced polymer backbone twisting influences the device characteristics of BHJ solar cells. The geometric structure, electronic and optical properties, charge-carrier mobilities, and photovoltaic characteristics of polymer:fullerene blends for a family of poly(hexylthiophene)s (both regioregular and regiorandom P3HT, PDHTT, and PDHBT, shown in Chart1) are systematically investigated.

Chart 1. Chemical Structures of P3HT[a], PDHTT, and PDHBT

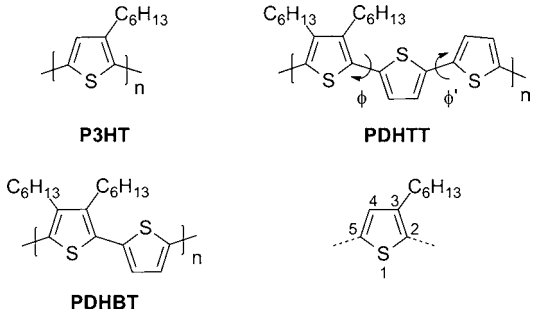

[a]Chemical structures of the two regiorandom P3HT analogues are provided in the Supporting Information. The atom numbering scheme is shown for reference.

Poly(3,4-dihexyl-2,2′:5′,2″-terthiophene) (PDHTT)[15,16] and poly(3,4-dihexyl-2,2′-bithiophene) (PDHBT)[17] contain dialkyl substituents on the 3- and 4-positions of thiophene with bi- and monothiophene spacers, respectively. We show that the 3,4-dialkyl substituents have a significant influence on the degree of backbone twisting both in solution, due to torsional strain, and in solid films, where the side-chain placement additionally influences the molecular packing and morphology.

Larger backbone twisting is found to increase the poly(hexylthiophene) IP, resulting in a larger V_{oc}. Reducing the average number of electron-donating alkyl substituents per thiophene ring in PDHTT additionally increases the IP and V_{oc}. Excessive backbone twisting, on the other hand, results in a reduced J_{sc} and fill factor due to an increase (blue shift) of the optical gap and lower hole mobility. A balance between these factors is reached with PDHTT, which has a relatively large diode hole mobility of 3×10^{-4} cm^2/V·s despite a lack of identifiable $\pi-\pi$ stacking in films. BHJ solar cells using PDHTT produce a V_{oc} that is 19% larger than P3HT devices (built herein) without a significant sacrifice of either the J_{sc} or fill factor, resulting in solar cell PCE of 4.2%.

RESULTS AND DISCUSSION

Synthesis. PDHTT[16] and PDHBT[17] contain dialkyl substituents on the 3- and 4-positions of thiophene with bi- and monothiophene spacers, respectively. The polymers were independently synthesized from the dialkyl substituted monomers by Stille polymerization (Supporting Information (SI)). Regioregular P3HT and regiorandom P3HT (RRa-P3HT) were purchased from Rieke Metals, Inc. We note that there may be small differences in purity among the studied polymers as the synthetic and purification procedures differ among the commercial sources[23] and the independently synthesized polymers (see SI).

As listed in Table 1, the number-averaged molecular weight for PDHTT is lower than for the other polythiophenes considered in this study since PDHTT has fewer solubilizing alkyl chains per thiophene ring (2/3) versus the other polythiophenes (1) and is consequently slightly less soluble.

Table 1. Number-Average Molecular Weights (M_n) and Polydispersity Index (PDI)

polymer	M_n (kDa)[a]	PDI
P3HT[b]	25	1.8
PDHTT	8.6	1.5
PDHBT	22	2.0
RRa-P3HT[b]	24.5	2.9

[a]Determined from GPC using THF as an eluent and polystyrenes as the standards. [b]Reported by Rieke Metals, Inc.

Structural Analysis. Density functional theory (DFT) calculations at the B3LYP/6-31G(d,p) level were carried out on a series of oligothiophene structures to investigate the influence of alkyl side-chain number and placement on twisting of the conjugated backbone. The results discussed here are for oligomers with similar conjugation path lengths (12 thiophene rings for each oligomeric structure as shown in Figure S1), and the geometric patterns reported are taken from the central portion of the structure so as to mitigate end effects. As expected, the differing substitution patterns along the oligothiophene backbone result in rather distinct differences in the (gas-phase) degree of twisting. P3HT has a calculated backbone twist of 21°, in agreement with previous results;[18,19] planarizing the system to give the fully planar form (the inferred thin-film structure) results in an energetic destabilization of 3.3 kcal/mol for the 12-ring oligomer (Figure S2). The asymmetric nature of the hexyl chain placement on the individual thiophene rings induces slight differences in the carbon−carbon bond lengths (C2−C3 = 1.393 Å, C3−C4 = 1.420 Å, and C4−C5 = 1.383 Å) within the ring, which in turn leads to a slight asymmetry in the bond-length alternation (BLA) pattern within the thiophene ring (0.037 and 0.027 Å).

dx.doi.org/10.1021/ja210954r | J. Am. Chem. Soc. 2012, 134, 5222−5232

For the two regiorandom P3HT structures considered (Figure S3), there is a notable difference in the twist angles, bond lengths, and BLA between the thiophene rings. In particular, the twist angles between the imposed head-to-head defects are larger than 65°, while the other thiophene−thiophene torsions are on the order of 15−25°, as in regioregular P3HT. Among the two regiorandom P3HT oligomers, RRa2-P3HT is the most energetically stable (by 1.2 kcal/mol).

For PDHTT and PDHBT, two symmetric structural forms of thiophene are present—unsubstituted and dihexyl-substituted. The carbon−carbon bonds in the dihexyl-substituted structure (C2−C3 ≈ 1.39 Å and C3−C4 ≈ 1.44 Å) are longer than their unsubstituted counterparts (C2−C3 ≈ 1.38 Å and C3−C4 ≈ 1.42 Å), and manifest a slightly larger BLA (~0.05 vs 0.03 Å). The twists within the PDHTT and PDHBT backbones between the substituted and unsubstituted structures is on the order of 30−40° (Figures S4 and S5); for PDHTT, the twist between the unsubstituted thiophene rings is 16°. We note that for PDHBT, *syn*- and *anti*-arrangements among the monomer units were investigated—in the case of the *syn*-conformer, the hexyl chains are on opposite sides of the backbone, while in the *anti*-conformer the hexyl chains are on the same side of the backbone; the *syn*-conformation is 1.4 kcal/mol more stable. Overall, the DFT calculations suggest that regioregular P3HT has the lowest degree of backbone twisting, while PDHTT, PDHBT, and the regiorandom P3HT oligomers are progressively more twisted across the entire length of the oligomer.

To estimate the energy barriers associated with the thiophene−thiophene torsions along the conjugated backbone, torsion energy profiles for four terthiophene derivatives were examined at the B3LYP/6-31G(d,p) level of theory,[20] shown in Chart 2 and Figure 1. The thiophene−thiophene twists of the

Chart 2. Terthiophene Chemical Structures

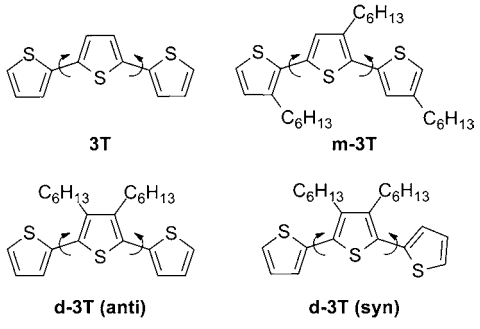

energy-minimized structures for the various terthiophenes are similar to those observed for the full oligomer structures. The energy required to planarize the unsubstituted (3T) and monohexyl-substituted (m-3T) terthiophenes falls well within thermal energy at room temperature (RT, 0.6 kcal/mol); these results are similar to those previously described for bithiophene.[21] Due to the steric interactions induced by the additional alkyl chain, the energetic requirements to planarize the dihexyl-substituted structures are 2.1−3.6 kcal/mol. Such energetic differences suggest that the polymers could pack in different manners in the solid state.

To examine the nature of the twisted dialkyl-substituted thiophene derivatives in more detail, a hexamer analogue of PDHTT (3′,4′,3‴,4‴,-tetrabutyl-2,2′:5′,2″:5″,2‴:5‴,2⁗:5⁗,2⁗⁗-hexathiophene) was synthesized and crystals grown for single-crystal X-ray analysis. The hexathiophene was synthesized via reported oxidative homocoupling,[22] where 3,4-dihexyl chains were truncated to 3,4-dibutyl chains to facilitate eventual crystal growth. Single crystals were obtained by slow diffusion of methanol in a solution of the sexithiophene derivative in chloroform.

Focusing on the central portion of the crystalline hexamer structure (Figure S6), the carbon−carbon bonds in the dihexyl-substituted thiophene (C2−C3 ≈ 1.37−1.39 Å and C3−C4 ≈ 1.44 Å) are longer than those in the unsubstituted thiophene (C2−C3 ≈ 1.36−1.38 Å and C3−C4 ≈ 1.42 Å), and manifest a slightly larger BLA (~0.06 vs 0.03 Å); these results are in good agreement with the calculated oligomer structure of PDHTT (Figure S6). The twists between the substituted and unsubstituted thiophenes are on the order of ~20°, while the central twist between the unsubstituted thiophenes is ~0° (as noted above, the energy to planarize unsubstituted thiophenes is smaller than RT). Notably, the twisted backbone of this hexathiophene contrasts with the previously reported coplanar backbone of the 3-butylthiophene pentamer as determined from XRD studies.[23] These twist angles, though, are smaller than those calculated for the isolated PDHTT oligomer, but fall in line with expectations of smaller torsions due to intermolecular packing forces in the crystal. Evaluation of the butyl-substituted hexamer at the B3LYP/6-31G** level of theory shows (nearly) identical geometric parameters (bond lengths, twist angles) to the hexyl-substituted PDHTT oligomer described above, indicating little-to-no influence imparted by the butyl versus the hexyl side chains. These results provide confidence in the accuracy of the geometric structures predicted by the model oligomers of the full polymer systems. Importantly, the observed twisted backbone demonstrates that the 3,4-dialkylthiophene unit should induce pronounced twists in the oligomer/polymer chain.

Thin-Film GIXS Characterization and Field-Effect Transistor Mobility. Grazing incidence X-ray scattering (GIXS) measurements were performed on thin films of P3HT, PDHTT, and PDHBT to investigate the packing structure of the polymers in as-cast and annealed films (Figure 2). The polymers containing the more twisted backbone structure, as determined by the DFT calculations, pack in a more disordered fashion and exhibit a lower degree of crystallinity. High-intensity scattering from lamellar $d(100)$ spacings are observed along the q_z direction for the P3HT films (15.8 Å in as-cast film and 16.0 Å in annealed film), with a strong in-plane diffraction pattern arising from the (010) peak that corresponds to $\pi-\pi$ stacking between the polymer backbone (3.83 Å in as-cast film and 3.81 Å in annealed film); such a diffraction pattern in an annealed film indicates that P3HT is mostly oriented with the polymer backbone edge-on with respect to the substrate surface ($\pi-\pi$ stacking direction parallel to the substrate).[15,24] With increasing backbone twist, isotropic rings near $q \approx 1.42$ Å^{-1} are more visible, indicating less ordered packing structure in as-cast films of PDHTT, PDHBT, and RRa-P3HT. Diffraction peaks from interlayer lamellar $d(100)$ spacings are also observed for PDHTT (19.2 Å in as-cast film and 19.0 Å in annealed film) and PDHBT (23.9 Å in as-cast film and 22.5 Å in annealed film).

Although diffraction peaks from lamellar $d(100)$ spacings are observed for PDHTT and PDHBT, the distinct scattering patterns from $\pi-\pi$ stacking near $q_{xy} \approx 1.7$ Å^{-1} are not observed. These results signify that the more twisted nature of the

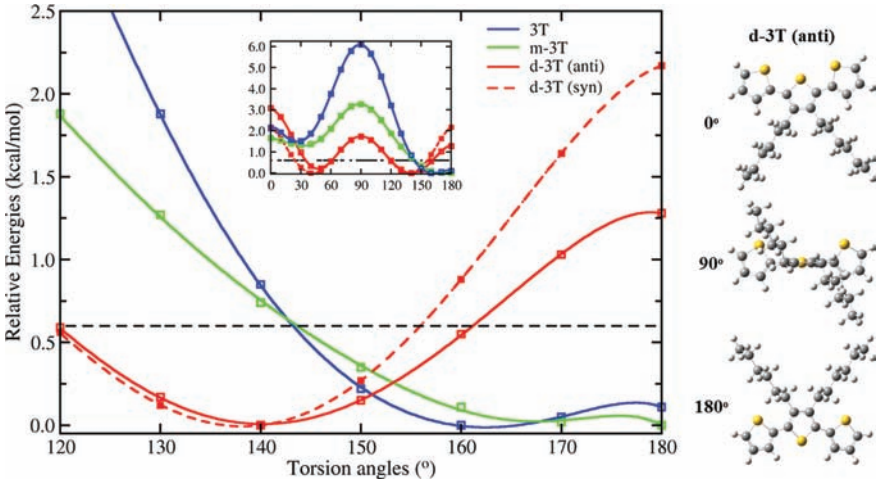

Figure 1. Thiophene−thiophene torsion potential energy surface for the four terthiophene derivatives as determined at the B3LYP/6-31G(d,p) level of theory. The inset shows the full potential energy surface, while the larger image focuses on the region around the minimum. The figures to the right illustrate the defined torsion angles.

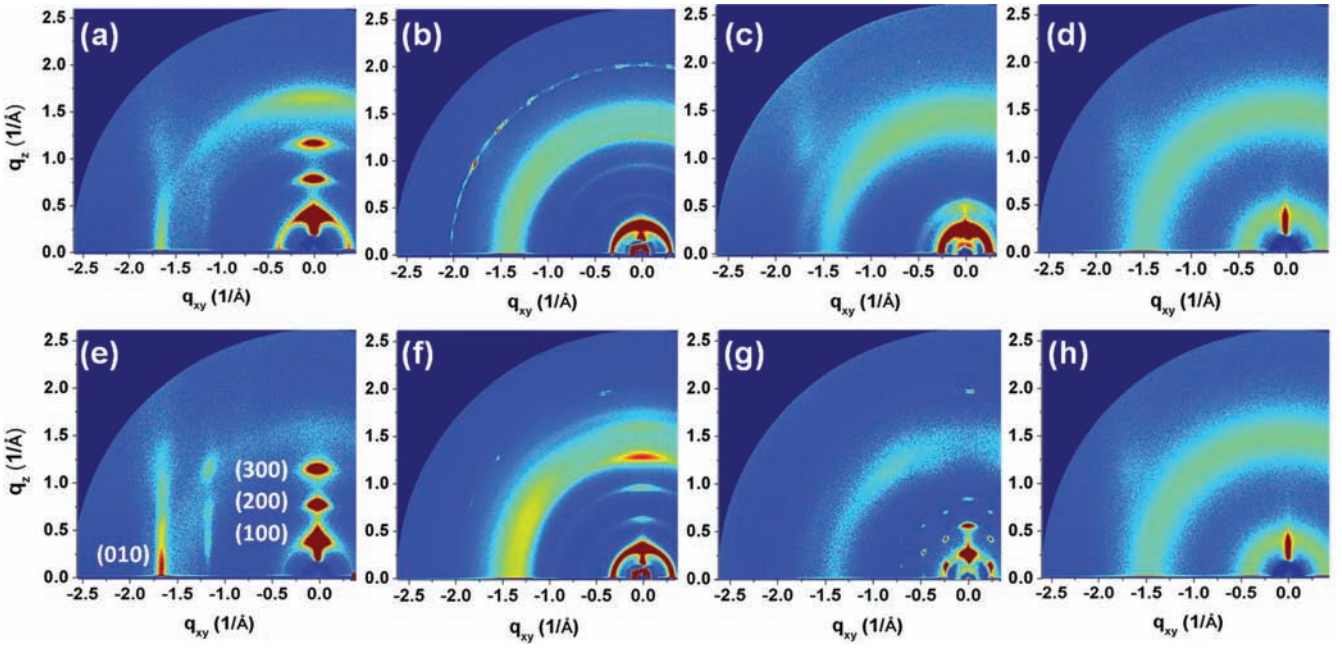

Figure 2. 2D GIXS images in films of (a) as-cast P3HT, (b) as-cast PDHTT, (c) as-cast PDHBT, (d) as-cast RRa-P3HT, (e) P3HT annealed at 225 °C, (f) PDHTT annealed at 210 °C, (g) PDHBT annealed at 225 °C, and (h) RRa-P3HT annealed at 225 °C.

polymer backbone leads to less ordered packing structures compared with P3HT; these results are consistent with the terthiophene torsion potential energy surfaces that revealed a considerably larger energetic requirement to planarize thiophene backbones containing dialkyl substitution. In addition, the longer lamellar *d*-spacings and lack of pronounced (010) scattering patterns from PDHTT and PDHBT films suggest that these polymers do not have the commonly observed edge-on packing structure; specifically, annealed PDHBT may adopt a hexagonal (cylindrical) lattice from the helical conformation caused by twisted hair-rod polymer backbones (see also Figure S5).[25−28] Precise peak indexing and visualizing packing structure within a unit cell are underway.

No obvious scattering patterns (corresponding to either *d*(100) or *d*(010)) were observed for the amorphous RRa-P3HT films (see also Figure S8). This indicates RRa-P3HT has the lowest degree of crystallinity and highest degree of backbone twisting among the studied polymers, in agreement with the DFT results.

A number of high-performance polymer semiconductors make use of 3-alkylthiophenes as the key monomer unit to promote side-chain interdigitation and strong $\pi-\pi$ stacking to provide lamellar packing in the solid state.[29−31] P3HT, with a high degree of regioregularity (>90% HT linkages) and an edge-on orientation (with respect to the substrate), has TFT mobilities of 0.05−0.2 $cm^2/V{\cdot}s$, while P3HT with low degrees of regioregularity shows mobilities of 10^{-4} $cm^2/V{\cdot}s$.[24] Previous studies with PDHTT revealed comparable mobilities to P3HT of up to 0.17 $cm^2/V{\cdot}s$ (μ_{avg} = 0.12 $cm^2/V{\cdot}s$) despite very weak $\pi-\pi$ stacking.[15] PDHBT has an average charge-carrier mobility of 2.6×10^{-4} $cm^2/V{\cdot}s$ (Figure S9).

As noted above, the 2D diffraction patterns of as-cast and annealed films (Figure 2) indicate that the PDHTT and PDHBT polymers have different packing structures from that

dx.doi.org/10.1021/ja210954r | J. Am. Chem. Soc. 2012, 134, 5222−5232

of P3HT. Although exact packing structures of PDHTT and PDHBT are not yet resolved, this result indicates that 3,4-dialkyl substituents are an effective way to modify the polymer packing structure, since comonomers can be easily varied for Stille polymerization with a 3,4-dialkylthiophene unit. This is analogous to the case of small conjugated oligomers where significant changes in packing motifs can be achieved by varying the substituent bulkiness. For example, the herringbone packing structure of pentacene and tetracene can be changed to a face-to-face π-stacking structure in the substituted molecules, 6,13-bis(triisopropyl-silylethylnyl)pentacene and 5,11-dichlorotetracene.[32−34]

Redox, Electronic Structure, and Optical Properties. Cyclic voltammetry (CV) was carried out to estimate the solid-state IP of the polymers in thin films deposited on Pt electrodes (see voltammograms in Figure S10). Onset oxidation potentials were determined relative to Fc/Fc^+, and the IP energies were estimated using 4.8 eV below vacuum level as the potential of Fc/Fc^+ (Table 2). The solid-state IPs systematically increase with the larger degree of backbone twist from 4.99 eV for P3HT to 5.15, 5.22, and 5.25 eV for PDHTT, PDHBT, and RRa-P3HT, respectively. We note that PDHTT has fewer electron-donating alkyl chains per thiophene ring compared to P3HT and PDHBT (2/3 vs 1), which has been previously suggested to influence polymer IPs (and the V_{oc} of polymer−fullerene BHJ solar cells).[4] While this indeed may have some influence on the varying IPs of the polymers studied here, it is important to recall that a delicate interplay exists between the side-chain density, the side-chain placement along the conjugated backbone, and the way in which steric interactions among the side chains influence the geometry (e.g., bond lengths, bond angles, and torsion angles) of the main chain. For instance, even though PDHBT and P3HT have the same density of alkyl side chains, the HOMO of the two longest oligomers studied here differ by ~0.2 eV (with the HOMO of planar PDHBT being more energetically stable, see SI) in enforced planar configurations.

The frontier molecular orbital energies for the oligomeric structures as determined at the B3LYP/6-31G(d,p) level of theory (molecular orbital iso-surfaces can be found in the SI) are listed in Table 2. The HOMO energies vary considerably with the twist angle along the oligothiophene backbone—ranging from −4.25 eV (P3HT) to −4.81 eV (PDHBT)—while the LUMOs fall within a narrower energetic range—from −1.81 eV (PDHBT) to −2.11 eV (P3HT); not surprisingly, the transport (fundamental) electronic gap (Δ_{HL}) increases with increasing twist angle in the P3HT analogues.

Introduction of the second hexyl chain and unsubstituted thiophene spacers in PDHTT and PDHBT induces a substantial energetic stabilization of the calculated HOMO energy versus (twisted) P3HT, corresponding with the increased twists within the oligothiopene backbone. However, unlike the P3HT structures, the LUMO energies are only slightly affected by the increased twist within the conjugated backbone, with the direction of the energetic shift differing between the two systems. In PDHBT, the more twisted nature of the oligothiophene backbone causes a slight energetic destabilization (−1.81 eV *syn*, −1.88 eV *anti*), in agreement with the influence of the degree of twisting within the P3HT series. On the other hand, the LUMO of PDHTT is stabilized (−2.05 eV) versus the twisted P3HT form and is similar to the LUMO energy of the fully planar P3HT (−2.11 eV) structure. This is a consequence of the delocalization of the PDHTT LUMO over the two more planar bithiophene units that neighbor each dialkyl-substituted thiophene. Overall, the HOMO energy trends across the oligomeric series are consistent with the polymer CV IPs.

Table 3 and Figure 3 depict the optical properties of P3HT, PDHTT, PDHBT, and RRa-P3HT, investigated both in solution (chlorobenzene) and thin films. P3HT, PDHTT and PDHBT have a similar absorption onset, while RRa-P3HT has a significantly larger optical gap (2.32 eV) in solution compared to the other polymers, a result in agreement with the large calculated twists in the backbone due to the head-to-head defects. A low-energy shoulder is observed in the PDHBT solution absorption spectra, and may be due to aggregation.[35]

Table 4 provides the vertical transition energy, transition dipole moment and oscillator strength, and electronic configurations of the lowest-lying excited states of the oligomeric structures as determined with time-dependent DFT (TDDFT) at the B3LYP/6-31G(d,p) level of theory. The $S_0 \rightarrow S_1$ transition energies increase in energy on going from P3HT (twisted 2.10 eV, planar 1.84 eV), to PDHTT (2.28 eV) and PDHBT (2.56 eV *syn*, 2.43 eV *anti*); the $S_0 \rightarrow S_1$ transition

Table 2. Solid-State Ionization Potentials Measured by Cyclic Voltammetry, Frontier Molecular Orbital Energies, and Twist Angles across the Thiophene Series Determined at the B3LYP/6-31G(d,p) Level of Theory[a]

polymer	IP(CV) (eV)[b]	HOMO (eV)	LUMO (eV)	Δ_{HL}	dihedral angle φ (°)
P3HT (twisted)	4.99	−4.43	−1.99	2.44	21
P3HT (planar)		−4.25	−2.11	2.14	0
PDHTT	5.15	−4.71	−2.05	2.66	30, 16
PDHBT (*syn*)	5.22	−4.81	−1.81	3.00	34
PDHBT (*anti*)		−4.71	−1.88	2.83	36
RRa-P3HT-1	5.25	−4.75	−1.83	2.92	~15—25, 65
RRa-P3HT-2		−4.59	−1.92	2.67	~15—25, 65

[a]Two conformations were examined for all of the polymers except PDHTT. Perspectives of the 3D structure for all of the conformations are shown in Figures S2−S5. [b]Ionization potentials were determined from CV using the onset of oxidation (E_{ox}^{onset}) of thin films spun from chloroform on platinum electrode in 0.1 M n-Bu_4NPF_6−acetonitrile solution and the conversion relationship IP (eV) = e (E_{ox}^{onset} + 4.8).

Table 3. Solution and Thin-Film Optical Properties for the Polythiophene Series

	solution[a]			thin film[b]			
polymer	λ_{max} (nm)	λ_{onset} (nm)	E_g^{opt} (eV)[c]	λ_{max} (nm)	λ_{onset} (nm)	E_g^{opt} (eV)[c]	absorption coefficient (cm^{-1})[e]
P3HT	464	557	2.23	553	652	1.90	1.8×10^5
PDHTT	477	563	2.20	508	632	1.96	1.7×10^5
PDHBT	463	559[d]	2.22[d]	511	596	2.08	1.8×10^5
RRa-P3HT	441	534	2.32	443	558	2.25	1.1×10^5

[a]Measured in solution in chlorobenzene. [b]Measured in films spun from chlorobenzene. [c]Optical gaps in the solution and thin films calculated from the onset of the absorption spectra. [d]Aggregation shoulder was excluded in absorption onset fitting. [e]Obtained using the equation = (optical density × ln 10)/thickness.

dx.doi.org/10.1021/ja210954r | J. Am. Chem. Soc. 2012, 134, 5222−5232

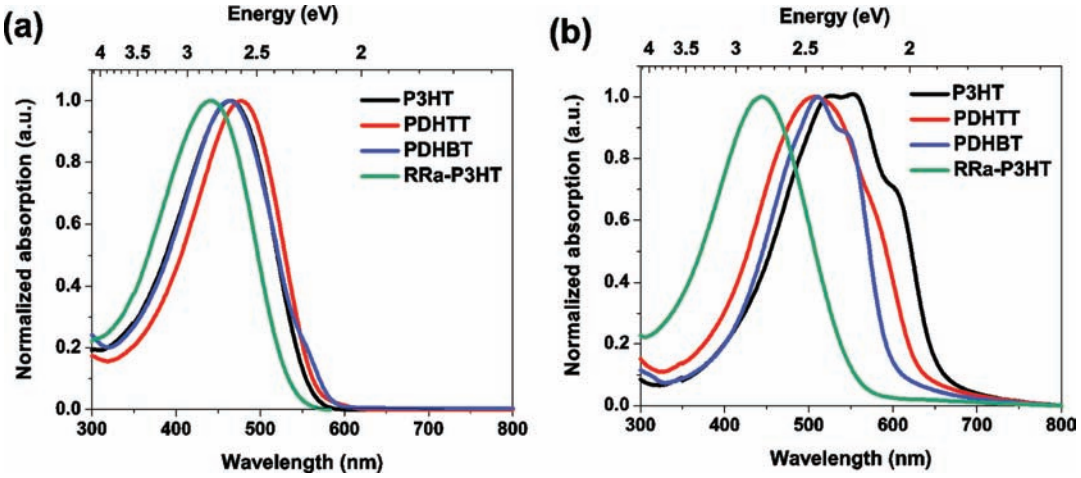

Figure 3. Normalized UV−vis spectra of polymers in (a) solution (chlorobenzene) and (b) films.

Table 4. TDDFT First Excited-State Vertical Transition Energies, Transition Dipole Moments, and Electronic Configurations As Determined at the B3LYP/6-31G(d,p) Level of Theory

		TDDFT			
polymer	conformation	E_{vert} (eV)[e]	μ_{ge} (D)	f_{ge}	electronic configuration
P3HT	twisted	2.10	21.35	3.62	HOMO→LUMO (94%); HOMO−1→LUMO+1 (4%)
	planar	1.84	24.00	4.03	HOMO→LUMO (93%); HOMO−1→LUMO+1 (3%)
PDHTT		2.28	20.18	3.52	HOMO→LUMO (91%); HOMO−1→LUMO+1 (6%)
PDHBT	*syn*	2.56	16.84	2.76	HOMO→LUMO (87%); HOMO−1→LUMO+1 (9%)
	anti	2.43	17.55	2.84	HOMO→LUMO (91%); HOMO−1→LUMO+1 (6%)
RRa-P3HT-1		2.33	18.45	3.01	HOMO→LUMO (96%); HOMO−1→LUMO+1 (2%)
RRa-P3HT-2		2.55	17.04	2.81	HOMO→LUMO (92%); HOMO−1→LUMO+1 (4%)

energies for the two regiorandom structures are 2.33 eV (RRa-P3HT-1) and 2.55 eV (RRa-P3HT-2). As noted above, these results are somewhat different from the solution data, in particular with regard to the slightly larger transition energy of PDHTT vs P3HT and PDHBT vs RRa-P3HT; it is expected that polarization effects and the variety of polymer conformations available in solution, along with the choice of oligomeric structure for the TDDFT calculations (in particular for the regiorandom P3HT structures), could lead to these modest discrepancies. These $S_0 \rightarrow S_1$ transitions are principally described as being HOMO→LUMO excitations, with very small contributions from a HOMO−1→LUMO+1 excitation. The ordering of the vertical transition energies correspond well with the transport gap energies, which are highly influenced by the twisting of the conjugated backbone and spatial arrangement of the wave functions.

In thin films, P3HT has the smallest optical gap (1.90 eV), followed by PDHTT (1.96 eV), PDHBT (2.08 eV), and RRa-P3HT (2.25 eV). The absorption spectrum of P3HT shows vibronic bands at 600 nm, which are typically attributed to ordered interplane interactions of the polymer backbones in the solid state.[36] These vibronic bands are weaker for PDHBT and are not present in either PDHTT or RRa-P3HT. The absorption profiles for each of the polythiophene thin films are red-shifted compared to those obtained in solution due to interchain electronic coupling. The size of the red-shift going from solution to thin-film correlates well with the optical gap of the polymer in the solid state and is larger for the smallest optical gap P3HT (0.33 eV) vs PDHTT (0.24 eV), PDHBT (0.14 eV), and RRa-P3HT (0.07 eV). The large variation in the red-shift from solution to thin-film suggests significant differences in the interchain interactions of the polymers and the ability for the polymers to pack in a dense, orderly fashion. For this polymer series, the ability of the polymers to pack in an orderly fashion, as evidenced by the GIXS measurements, correlates with the degree of polymer twisting and leads to changes to the polymer optical gaps in thin films due to interchain interactions and possible changes in the backbone twisting. This suggests an interplay between the polymer backbone twisting and the solid film packing structure: torsional twisting of individual polymer chains influences the solid-state packing structures that the polymer can form when the chains aggregate together, which in turn influences the final twisting of the polymer backbone in solid films. The particularly large red-shift of the P3HT film absorption can be explained by the ability of the chains to pack in a compact fashion that causes the thiophene rings to be more coplanar in the solid state than in solution. This orderly packing motif is not available to the other polymers, which need to remain twisted in order to fill space. A smaller film peak absorption coefficient of RRa-P3HT was observed which may be a consequence of a reduction in conjugation length and interchain interactions of RRa-P3HT compared to the other polymers due to a larger degree of backbone twisting.

Solar Cell Properties and Diode Hole Mobilities. The photovoltaic properties of P3HT, PDHTT, PDHBT, and RRa-P3HT were investigated in the device structure ITO/PEDOT:PSS/polymer:$PC_{71}BM$/Ca/Al, with the active layers spun from chlorobenzene. Hole-only diodes were fabricated with the same device structure but using a top gold contact. Optimized P3HT-, PDHTT-, and PDHBT-based solar cells were obtained with weight ratios of 1:0.8 (polymer:$PC_{71}BM$),

dx.doi.org/10.1021/ja210954r | J. Am. Chem. Soc. 2012, 134, 5222−5232

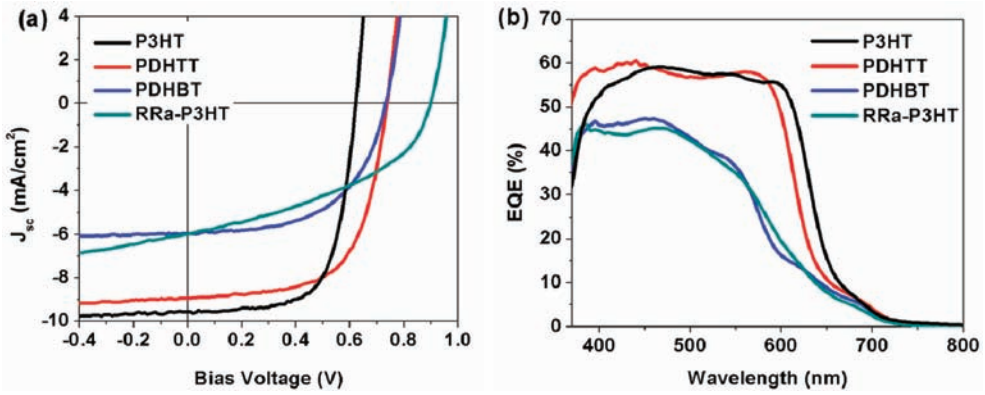

Figure 4. (a) Current–voltage plots under illumination with AM 1.5G solar simulated light (100 mW/cm^2) and (b) EQE spectra of the BHJ solar cells of P3HT, PDHTT, PDHBT, and RRa-P3HT with $PC_{71}BM$.

while an optimal blend ratio of 1:4 was found for the RRa-P3HT devices. J–V curves and lower external quantum efficiency (EQE) spectra are shown in Figure 4, while the optimized device characteristics are summarized in Table 5.

Solar cells made with PDHTT and PDHBT exhibit V_{oc}'s that are more than 0.1 V larger than the corresponding P3HT devices. This voltage improvement is primarily attributable to the larger IP of the two polymers, a direct consequence of the increased twist in the conjugated backbone. The PDHTT devices have a slightly smaller J_{sc} than the P3HT devices, due to the larger optical gap. Combined with similar fill factors between the PDHTT and P3HT devices, these parameters result in a slight PCE improvement for PDHTT (4.20%) versus P3HT (4.00%). In contrast, the more twisted PDHBT and RRa-P3HT have a significantly lower J_{sc}, both due to their larger optical gap and lower EQE spectrum over all wavelengths.

Table 5. Photovoltaic Properties of Highest Efficiency Polymer Solar Cells Blended with $PC_{71}BM$

polymer	blend ratio	J_{sc} (mA/cm^2)	V_{oc} (V)	fill factor	PCE_{max} (PCE_{avg}) (%)
P3HT	1:0.8	9.57	0.620	0.67	4.00 (3.92)[a]
PDHTT	1:0.8	8.93	0.735	0.64	4.20 (4.01)
PDHBT	1:0.8	5.96	0.745	0.65	2.87 (2.68)[b]
RRa-P3HT	1:4	5.99	0.900	0.42	2.27 (2.21)

[a]Annealed at 150 °C for 30 min. [b]Annealed at 110 °C for 10 min.

The optimal device thickness systematically decreases with increased twisting of the polymer backbone (Table 6). To determine if hole extraction is being impeded in devices employing the more twisted polythiophenes, hole mobilities were estimated from space-charge-limited current measurements on hole-only diodes of the polymer:fullerene blends.[37] The hole mobility of the PDHTT blend is similar to that of P3HT, while the more twisted backbones of PDHBT and RRa-P3HT result in hole mobilities that are 0.5 and 1 order of magnitude smaller, respectively.

The differences in hole mobility can also explain the reduction in internal quantum efficiency (IQE) for devices containing the more twisted PDHBT and RRa-P3HT polymers. The internal quantum efficiency is calculated by taking into account optical interference effects and parasitic absorptions in the electrodes.[38] The calculated IQE is relatively wavelength independent for the PDHTT, PDHBT, and RRa-P3HT devices (Figure 5). The IQE is smaller at shorter wavelengths for the P3HT devices. This has been previously reported for P3HT:$PC_{61}BM$ blend devices cast from dichlorobenzene, and was attributed to the recombination of excitons formed in the large fullerene domains that are not able to diffuse to the heterojunction.[39] Since the optimal PDHTT, PDHBT, and RRa-P3HT devices were not annealed, or annealed at lower temperatures for less time than the P3HT devices, the fullerene domains in these devices are likely smaller than in the P3HT devices, resulting in a wavelength independent IQE. The IQE is similar at longer wavelengths (>500 nm) for the large-mobility polymers P3HT and PDHTT, but about 10% smaller for the more twisted polymers PDHBT and RRa-P3HT. This suggests that the reduced hole extraction ability of PDHBT and RRa-P3HT is responsible for a reduction in both the optimal

Table 6. Hole Mobility, Optimized Thickness, and Internal Quantum Efficiency

polymer	μ_h (cm^2/V·s)[a]	thickness (nm)	fill factor[c]	IQE (%)[b]	J_{sc} (mA/cm^2)[c]
P3HT	3×10^{-4}	225	0.66	67	9.56
PDHTT	3×10^{-4}	165	0.66	67	8.54
PDHBT	7×10^{-5}	105	0.61	55	5.87
RRa-P3HT	2×10^{-5}	65	0.41	57	5.97

[a]Space charge limited hole mobility measured for hole only diodes. [b]Wavelength-averaged internal quantum efficiency accounting for optical interference effects and parasitic absorptions in the electrodes. [c]Average values.

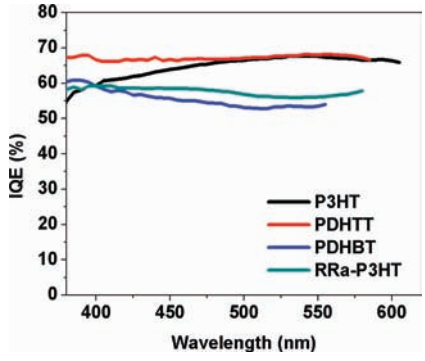

Figure 5. IQE spectra for the various polymer:$PC_{71}BM$ devices.

dx.doi.org/10.1021/ja210954r | J. Am. Chem. Soc. 2012, 134, 5222–5232

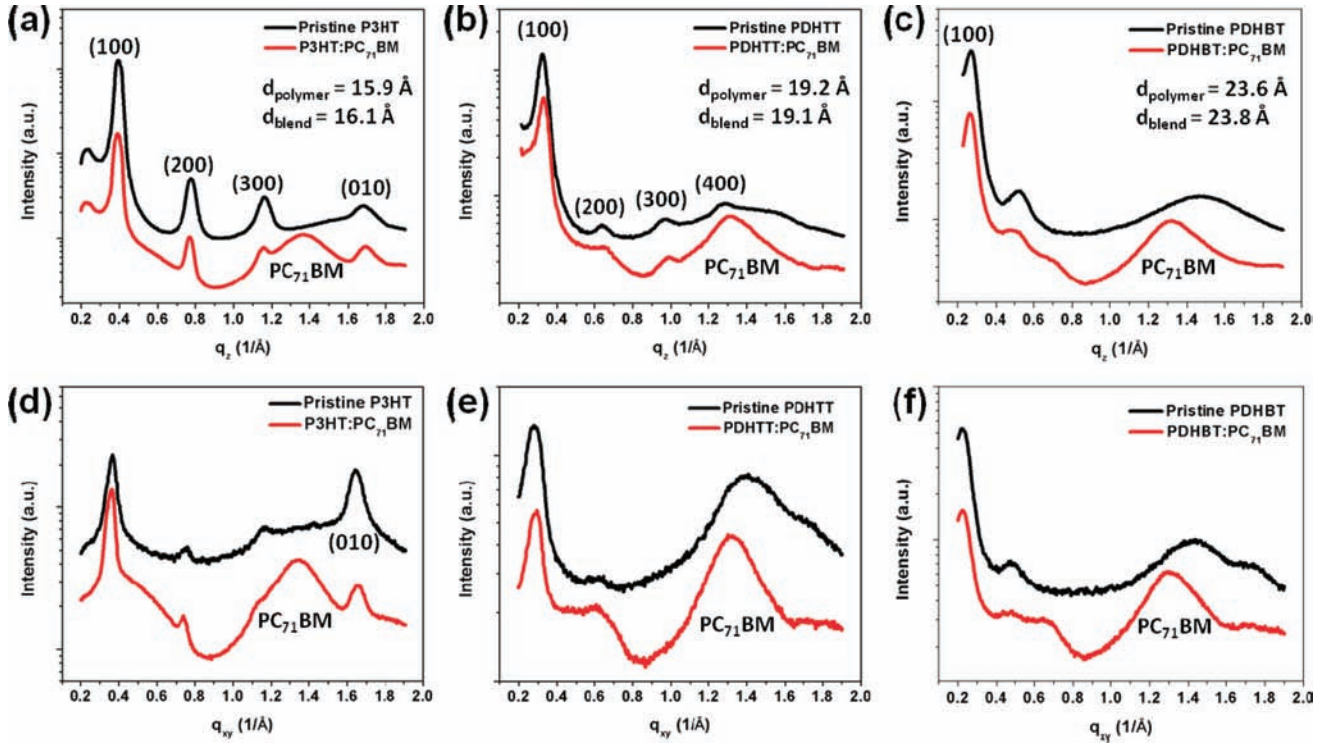

Figure 6. (a–c) Out-of-plane and (d–f) in-plane diffraction plots extracted from 2D GIXS patterns of polymer and polymer:$PC_{71}BM$ blends for (a,d) P3HT, annealed at 150 °C for 30 min, (b,e) PDHTT, as cast, and (c,f) PDHBT, annealed at 110 °C for 10 min.

thickness and IQE, resulting in the lower EQE for these devices.

The placement of the side chains also was found to have a significant impact on the optimal polymer:fullerene blend ratio for solar cell performance. Previous studies have found that fullerene molecules can intercalate between the side chains of several polymers (which have sufficient spacing between the side chains to accommodate a fullerene molecule), as evidenced by an increase in the lamellar *d*-spacing of the polymer blend film compared to the pure polymer.[40,41] Polymers in which intercalation was observed produced solar cells at an optimal blend ratio of roughly 1:4 (polymer:fullerene), while those that do not undergo intercalation (such as P3HT) optimize around 1:1. For the polythiophenes in this study, the lamellar (100) *d*-spacing derived from GIXS studies is almost the same in the neat films as in the blends (Figure 6). This indicates that there is no intercalation between fullerene and PDHTT or PDHBT. The lack of intercalation for the PDHTT and PDHBT blends is consistent with the optimal blend ratio of 1:0.8 for photovoltaic devices containing these materials (Table 5). The optimal ratio of 1:4 for the RRa-P3HT:$PC_{71}BM$ devices suggests intercalation likely occurs in these blends, though this could not be verified by GIXS due to the lack of clear scattering contributions from the amorphous polymer film (see Figure S8).

Charge-Transfer States and Polymer–Fullerene Coupling. We have shown in previous sections that polymers with more twisted backbones exhibit a larger IP, resulting in devices with larger V_{oc}. Several reports have suggested that reducing polymer–fullerene electronic interactions can also increase V_{oc} by reducing the dark current and radiative recombination losses.[14,42,43] To determine if the large V_{oc}'s in the devices made from the more twisted polymers are partly due to a decrease in polymer–fullerene coupling, we examined the charge-transfer (CT) states of each of the polymer:fullerene blends. Excited-state CT complexes are weakly bound excitons at the polymer:fullerene interface. Since CT excitons are believed to be immediate precursors to free carriers, the V_{oc} of BHJ solar cells has been shown to depend linearly on the CT energy (E_{CT}).[42−45] According to the detailed balanced model proposed by Vandewal et al.,[42,43] which expands on the work of Rau,[46] the difference between E_{CT}/q and V_{oc} provides a measurement of the radiative and nonradiative recombination in the device, where $-q$ is the charge of an electron. Devices with stronger coupling between the polymer and fullerene are thus expected to have a larger difference between E_{CT}/q and V_{oc} due to increased losses from radiative recombination and dark current.

The energy of CT complexes can be determined by measuring the absorption spectra or EQE spectra of the polymer:fullerene blend. The absorption coefficient for directly exciting CT states at the interface is typically low (10^2–10^3 cm^{-1}) and requires sensitive detection techniques, such as photothermal deflection spectroscopy (PDS).[47,48] The photocurrent produced by directly exciting CT states can also be detected in BHJ devices using an optical chopper and lock-in amplifier (Figure 7). A small contribution to the EQE spectra below the absorption onset of the polymers and fullerenes (<1.55 eV) is observed, which is attributed to photocurrent generated from excitation of the CT state. This feature in the EQE spectrum is also observed in the absorption spectrum of blend films, but not present in the absorption of the pure polymers or fullerene, as measured by PDS (Figure S11). A representative value for E_{CT} for each device can be obtained using Marcus theory and assuming a Gaussian distribution of

dx.doi.org/10.1021/ja210954r | J. Am. Chem. Soc. 2012, 134, 5222–5232

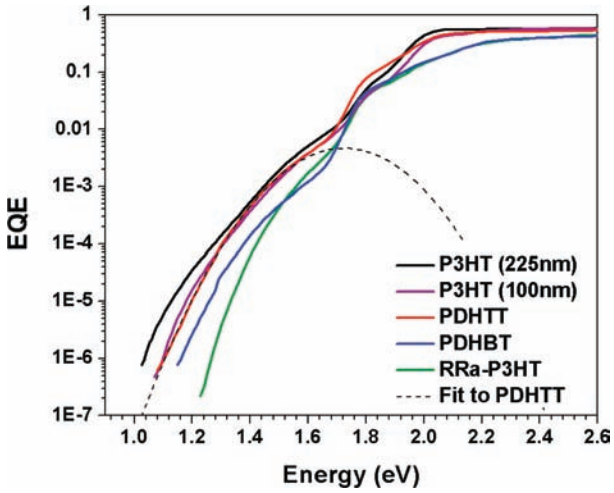

Figure 7. EQE spectra vs photon energy of optimized polymer–fullerene devices and an example fit of sub-bandgap region to eq 1 for measuring E_{CT}. The EQE spectrum for a thinner-than-optimal (100 nm) P3HT device is also shown, which exhibits a narrower CT state distribution than the thicker (225 nm) P3HT devices.

CT states by fitting the low energy portion of the EQE spectra ($EQE_{PV}(E)$) with eq 1:[42]

$$EQE(E) \propto \frac{1}{E\sqrt{4\pi\lambda kT}} \exp\left(-\frac{(E_{CT}+\lambda-E)^2}{4\lambda kT}\right) \quad (1)$$

Here, k denotes the Boltzmann constant, T is the temperature, and λ is related to the width of the CT absorption and reorganization energy of the CT state.[42] The EQE spectra of the devices are shown in Figure 7 on a logarithmic scale, while the fitted values for E_{CT} are presented in Table 7.

A strong linear correlation is observed between the E_{CT}, V_{oc}, and polymer IP. For the PDHTT, PDHBT, and RRa-P3HT devices, the V_{oc} is roughly 0.57 V less than the measured CT potentials, E_{CT}/q (Figure 8). This voltage loss is comparable to other polymer:fullerene BHJ devices, whose losses fall in the range of 0.53–0.59 V.[42] The CT photocurrent spectrum is significantly broader and red-shifted for the optimized (225 nm thick) P3HT devices, suggesting a broader and lower distribution of CT state energies which has been shown to be due to fullerene aggregation.[51] Equation 1 could not accurately describe the shape of the entire CT contribution to the EQE spectra for these devices. Consequently there may be some error in the value of E_{CT} =1.14 eV determined from fitting only the lowest energy portion of the spectra, which would explain why the apparent difference between the fitted E_{CT}/q and V_{oc} (0.52 V) is smaller for the P3HT devices.

Table 7. Solid-State Polymer IPs, CT Energies, and Average V_{oc} of the Solar Cell Devices

polymer	IP(CV) (eV)[a]	E_{CT} (eV)[b]	$E_{CT,DFT}$ (eV)[c]	V_{oc} (V)[d]
P3HT	4.99	1.14[e]	1.49	0.622[e]
PDHTT	5.15	1.30	1.69	0.712
PDHBT	5.22	1.32	1.84	0.748
RRa-P3HT	5.25	1.45	1.93	0.891

[a]IPs measured by cyclic voltametry. [b]Charge-transfer state energy measured by fitting the sub-bandgap region of the EQE spectra to eq 1. [c]Singlet $E_{CT,DFT}$ calculated using the constrained DFT formalism[49] at the B3LYP/6-31G(d,p) level and the continuum solvation conductor-like screening model[50] with a dielectric constant (ε) of 3. Note that the acceptor used in the calculated E_{CT} is C_{60}. [d]Average measured open-circuit voltage. [e]Measured for 225 nm thick devices.

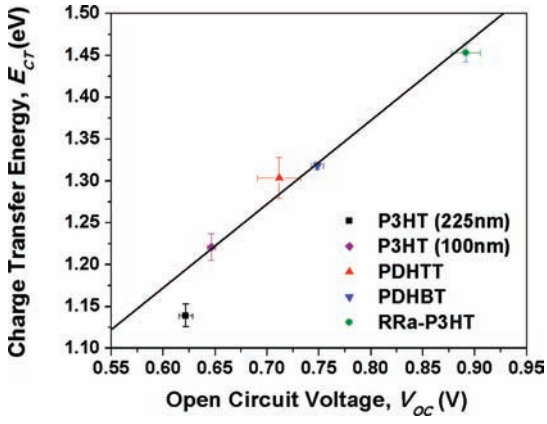

Figure 8. Charge-transfer energy (E_{CT}) determined from EQE measurements fit to eq 1, versus V_{oc}. The solid line represents a loss of 0.57 V between the CT state potential and V_{oc}.

Interestingly, when the P3HT devices are spun from a more dilute solution and made thinner (~100 nm), there is both a significant narrowing of the CT contribution to the EQE spectra and an increase in the measured V_{oc} and fitted E_{CT}. The difference between E_{CT}/q and V_{oc} for the thin P3HT devices is the same (0.57 V) as for the PDHTT, PDHBT, and RRa-P3HT devices. The decrease in V_{oc} and E_{CT} and broadening of the CT state distribution in the thick devices is likely an indication of larger phase segregation in the blend film morphology. The morphology and length scale of horizontal and vertical phase segregation in P3HT:PCBM blends has been shown to depend on film thickness due to thickness-dependent kinetics of solvent evaporation and crystallization.[52] A similar change in V_{oc} and the CT state distribution was reported for annealed P3HT:PCBM and MDMO-PPV:PCBM blend devices and was attributed to the formation of PCBM clusters which stabilize the CT states.[51] A coarser morphology in the thick P3HT devices may also result in larger spatial variations in the local dielectric constant and degree of crystallinity of the P3HT, which could produce the observed inhomogeneous CT state broadening. The same drop in potential of 0.57 V between the E_{CT}/q and V_{oc} for the entire family of poly(hexylthiophene)s suggests that the total impact of radiative and nonradiative losses on V_{oc} is similar for all of the polymers. Assuming nonradiative recombination (which is related to the electroluminescence efficiency) is similar within this family of polymers:fullerene blends, this implies that there are no significant differences in either the electronic coupling or radiative recombination losses due to polymer twisting.

DFT methods were also employed to evaluate both the CT state energy ($E_{CT,DFT}$) and the effective electronic coupling between the model oligomers and fullerene (for simplicity, C_{60} was used to represent the fullerene in the donor–acceptor complex) (Tables S6 and S7). To determine the complex geometry, the pentagonal face of C_{60} was placed parallel to the plane of the central unsubstituted thiophene unit in PDHTT and PDHBT or hexyl-substituted thiophene unit in P3HT. Grimme's dispersion-corrected B97D functional[53] and a 6-31G(d,p) basis set was used to determine the binding energy of the complex as the oligomer–C_{60} distance was varied from 2.8

dx.doi.org/10.1021/ja210954r | J. Am. Chem. Soc. 2012, 134, 5222–5232

to 4.4 Å (Figures S12–S14). The largest binding-energy configuration was then used to evaluate both the CT state energy and effective electronic coupling. As could be expected, the largest binding energy for the complex is calculated to shift to larger oligomer–fullerene distances with increased twist within the conjugated backbones; across the series, the oligomer–fullerene distances ranged from 3.15 to 3.25 Å.

Based on these complex geometries, $E_{CT,DFT}$ was evaluated by employing the constrained DFT formalism[49] at the B3LYP/6-31G(d,p) level coupled with the continuum solvation conductor-like screening model (Table 7 and Table S7).[50] Overall, the $E_{CT,DFT}$ values correspond well with those determined by the EQE measurements, though the absolute values of $E_{CT,DFT}$ are overestimated by 0.3–0.5 eV. The overestimation of the CT state energy could come from a variety of sources, including differences in the dielectric constants between the donor and acceptor at the interface, the simplicity of taking into account only a two-molecule complex, and the potential for underestimation of the CT state energies in the EQE measurements.

The effective electronic couplings between the HOMOs of the oligothiophenes and the triply degenerate LUMO of C_{60} have been calculated at the B3LYP/6-31G(d,p) level using the fragment orbital approach.[54] As the twist within the oligomer conjugated backbone increases, the increased distance between the oligomer and C_{60} leads to a reduced electronic coupling between the oligomer and fullerene. Although this correlates well with the increase in V_{oc} with increased twisting in the polymer backbone, the variation in the electronic coupling is quite small and results in an estimated icrease in V_{oc} of 16, 28, and 19 mV for PDHTT, PDHBT, and RRa-P3HT, respectively, compared with P3HT (see SI). These values are roughly one-order of magnitude smaller than the observed increases in V_{oc}. Consequently, the differences in V_{oc} appear primarily attributable to the differences in the polymer IP versus differences in electronic coupling.

CONCLUSION

We have demonstrated that side-chain-induced twisting of the poly(alkylthiophene)-conjugated backbone can have an important effect on the energetic and photogeneration properties of poly(alkylthiophene):fullerene BHJ solar cells. Although minimized torsions along the conjugated backbone are important for increasing delocalization along the conjugated backbone, which in turn can decrease the optical gap and increase the polymer hole mobility so as to achieve large photocurrents, optimal devices were surprisingly not those built from the P3HT polymer with the least degree of backbone twisting. Rather there exists an optimal balance (PDHTT) in the degree of polymer backbone twisting that increases the IP and enhances the V_{oc}, while not appreciably sacrificing photocurrent for the family of polymers considered. We note that devices based on polymers with sufficiently large IP's or smaller hole-carrier mobilities than polythiophenes may not benefit from more twisted backbone structures. Side-chain placement modifications provide a simple synthetic method to tune the degree of backbone twisting in polymer backbones for the optimization of organic electronic devices.

ASSOCIATED CONTENT

Supporting Information

Experimental details, synthesis of monomers and polymers, device preparation and characterization, optimized geometry of oligomer analogues, and electronic coupling between oligomer and fullerene. This material is available free of charge via the Internet at http://pubs.acs.org.

AUTHOR INFORMATION

Corresponding Author

zbao@stanford.edu

Notes

The authors declare no competing financial interest.

ACKNOWLEDGMENTS

This publication was partially based on work supported by the Center for Advanced Molecular Photovoltaics, Award No. KUS-C1-015-21, made by King Abdullah University of Science and Technology (KAUST). Portions of this research were carried out at the Stanford Synchrotron Radiation Lightsource user facility operated by Stanford University on behalf of the U.S. Department of Energy, Office of Basic Energy Sciences. Computational resources were partly made available through the CRIF Program of the NSF (Award No. CHE-0946869). E.T.H. was supported by the Fannie and John Hertz Foundation. We thank Michael F. Toney and Eric Verploegen for helpful discussions.

REFERENCES

(1) Press release, Konarka, November 29, 2010.
(2) Blouin, N.; Michaud, A.; Gendron, D.; Wakim, S.; Blair, E.; Neagu-Plesu, R.; Belletete, M.; Durocher, G.; Tao, Y.; Leclerc, M. *J. Am. Chem. Soc.* **2008**, *130*, 732–742.
(3) Chen, H. Y.; Hou, J. H.; Zhang, S. Q.; Liang, Y. Y.; Yang, G. W.; Yang, Y.; Yu, L. P.; Wu, Y.; Li, G. *Nat. Photon.* **2009**, *3*, 649–653.
(4) Hou, J.; Chen, T. L.; Zhang, S.; Huo, L.; Sista, S.; Yang, Y. *Macromolecules* **2009**, *42*, 9217–9219.
(5) Liang, V. Y.; Feng, D. Q.; Guo, J. C.; Szarko, J. M.; Ray, C.; Chen, L. X.; Yu, L. P. *Macromolecules* **2009**, *42*, 1091–1098.
(6) Gadisa, A.; Svensson, M.; Andersson, M. R.; Inganas, O. *Appl. Phys. Lett.* **2004**, *84*, 1609–1611.
(7) Zhou, E. J.; Cong, J. Z.; Yamakawa, S.; Wei, Q. S.; Nakamura, M.; Tajima, K.; Yang, C. H.; Hashimoto, K. *Macromolecules* **2010**, *43*, 2873–2879.
(8) Zou, Y.; Sang, G.; Wu, W.; Liu, Y.; Li, Y. *Synth. Met.* **2009**, *159*, 182–187.
(9) Li, Y. W.; Xue, L. L.; Xia, H. J.; Xu, B.; Wen, S. P.; Tian, W. J. *J. Polym. Sci., Part A: Polym. Chem.* **2008**, *46*, 3970–3984.
(10) Palayangoda, S. S. M., R.; Shah, B. K.; Neckers, D. C. *J. Org. Chem.* **2007**, *72*, 6584–6587.
(11) Rieger, R.; Beckmann, D.; Mavrinskiy, A.; Kastler, M.; Müllen, K. *Chem. Mater.* **2010**, *22*, 5314–5318.
(12) Szarko, J. M.; Guo, J.; Liang, Y.; Lee, B.; Rolczynski, B. S.; Strzalka, J.; Xu, T.; Loser, S.; Marks, T. J.; Yu, L.; Chen, L. X. *Adv. Mater.* **2010**, *22*, 5468–5472.
(13) Andersson, M. R.; Thomas, O.; Mammo, W.; Svensson, M.; Theander, M.; Inganas, O. *J. Mater. Chem.* **1999**, *9*, 1933–1940.
(14) Perez, M. D.; Borek, C.; Forrest, S. R.; Thompson, M. E. *J. Am. Chem. Soc.* **2009**, *131*, 9281–9286.
(15) Ko, S.; Verploegen, E.; Hong, S.; Mondal, R.; Hoke, E. T.; Toney, M. F.; McGehee, M. D.; Bao, Z. *J. Am. Chem. Soc.* **2011**, *133*, 16722–16725.
(16) Belletete, M.; Mazerolle, L.; Desrosiers, N.; Leclerc, M.; Durocher, G. *Macromolecules* **1995**, *28*, 8587–8597.
(17) Kokubo, H.; Sato, T.; Yamamoto, T. *Macromolecules* **2006**, *39*, 3959–3963.
(18) DeLongchamp, D. M.; Kline, R. J.; Lin, E. K.; Fischer, D. A.; Richter, L. J.; Lucas, L. A.; Heeney, M.; McCulloch, I.; Northrup, J. E. *Adv. Mater.* **2007**, *19*, 833–837.
(19) Northrup, J. E. *Phys. Rev. B* **2007**, *76*, 245202.

(20) For the m-3T structure, an additional torsional constraint was employed for the dihedral angle between the thiophene ring and side chain to keep the side chains in a similar position as the P3HT oligomer.
(21) Raos, G.; Famulari, A.; Marcon, V. *Chem. Phys. Lett.* **2003**, *379*, 364−372.
(22) Pappenfus, T. M.; Mann, K. R. *Inorg. Chem.* **2001**, *40*, 6301−6307.
(23) Chen, T. A.; Wu, X. M.; Rieke, R. D. *J. Am. Chem. Soc.* **1995**, *117*, 233−244.
(24) Sirringhaus, H.; Brown, P. J.; Friend, R. H.; Nielsen, M. M.; Bechgaard, K.; Langeveld-Voss, B. M. W.; Spiering, A. J. H.; Janssen, R. A. J.; Meijer, E. W.; Herwig, P.; de Leeuw, D. M. *Nature* **1999**, *401*, 685−688.
(25) Ballauff, M. *Angew. Chem., Int. Ed.* **1989**, *28*, 253−267.
(26) Knaapila, M.; Stepanyan, R.; Lyons, B. P.; Torkkeli, M.; Monkman, A. P. *Adv. Funct. Mater.* **2006**, *16*, 599−609.
(27) White, J. W.; Holt, S. A.; Foran, G. J. *Langmuir* **1999**, *15*, 2540−2542.
(28) Knaapila, M.; Stepanyan, R.; Lyons, B. P.; Torkkeli, M.; Hase, T. P. A; Serimaa, R.; Guntner, R.; Seeck, O. H.; Scherf, U.; Monkman, A. P. *Macromolecules* **2005**, *38*, 2744−2753.
(29) Ong, B. S.; Wu, Y. L.; Liu, P.; Gardner, S. *J. Am. Chem. Soc.* **2004**, *126*, 3378−3379.
(30) Mcculloch, I.; Heeney, M.; Bailey, C.; Genevicius, K.; Macdonald, I.; Shkunov, M.; Sparrowe, D.; Tierney, S.; Wagner, R.; Zhang, W. M.; Chabinyc, M. L.; Kline, R. J.; Mcgehee, M. D.; Toney, M. F. *Nat. Mater.* **2006**, *5*, 328−333.
(31) Osaka, I.; Zhang, R.; Sauve, G.; Smilgies, D. M.; Kowalewski, T.; McCullough, R. D. *J. Am. Chem. Soc.* **2009**, *131*, 2521−2529.
(32) Mattheus, C. C.; de Wijs, G. A.; de Groot, R. A.; Palstra, T. T. M. *J. Am. Chem. Soc.* **2003**, *125*, 6323−6330.
(33) Lee, K.; Kim, J. Y.; Park, S. H.; Kim, S. H.; Cho, S.; Heeger, A. J. *Adv. Mater.* **2007**, *19*, 2445−2449.
(34) Moon, H.; Zeis, R.; Borkent, E. J.; Besnard, C.; Lovinger, A. J.; Siegrist, T.; Kloc, C.; Bao, Z. N. *J. Am. Chem. Soc.* **2004**, *126*, 15322−15323.
(35) Kokubo, H.; Sato, T.; Yamamoto, T. *Macromolecules* **2006**, *39*, 3959−3963.
(36) Mauer, R.; Kastler, M.; Laquai, F. *Adv. Funct. Mater.* **2010**, *20*, 2085−2092.
(37) Goh, C.; Kline, R. J.; McGehee, M. D.; Kadnikova, E. N.; Frechet, J. M. J. *Appl. Phys. Lett.* **2005**, *86*, 122110−13.
(38) Burkhard, G. F.; Hoke, E. T.; McGehee, M. D. *Adv. Mater.* **2010**, *22*, 3293−3297.
(39) Burkhard, G. F.; Hoke, E. T.; Scully, S. R.; McGehee, M. D. *Nano Lett.* **2009**, *9*, 4037−4041.
(40) Mayer, A. C.; Toney, M. F.; Scully, S. R.; Rivnay, J.; Brabec, C. J.; Scharber, M.; Koppe, M.; Heeney, M.; McCulloch, I.; McGehee, M. D. *Adv. Funct. Mater.* **2009**, *19*, 1173−1179.
(41) Cates, N. C.; Gysel, R.; Beiley, Z.; Miller, C. E.; Toney, M. F.; Heeney, M.; McCulloch, I.; McGehee, M. D. *Nano Lett.* **2009**, *9*, 4153−4157.
(42) Vandewal, K.; Tvingstedt, K.; Gadisa, A.; Ingan; auml, s, O.; Manca, J. V. *Phys. Rev. B* **2010**, *81*, 125204.
(43) Vandewal, K.; Tvingstedt, K.; Gadisa, A.; Inganas, O.; Manca, J. V. *Nat. Mater.* **2009**, *8*, 904−909.
(44) Deibel, C.; Strobel, T.; Dyakonov, V. *Adv. Mater.* **2010**, *22*, 4097−4111.
(45) Veldman, D.; Meskers, S. C. J.; Janssen, R. A. J. *Adv. Funct. Mater.* **2009**, *19*, 1939−1948.
(46) Rau, U. *Phys. Rev. B* **2007**, *76*, 085303.
(47) Goris, L.; Poruba, A.; Hod'akova, L.; Vanecek, M.; Haenen, K.; Nesladek, M.; Wagner, P.; Vanderzande, D.; De Schepper, L.; Manca, J. V. *Appl. Phys. Lett.* **2006**, *88*, 05113.
(48) Holcombe, T. W.; Norton, J. E.; Rivnay, J.; Woo, C. H.; Goris, L.; Piliego, C.; Griffini, G.; Sellinger, A.; Bredas, J. L.; Salleo, A.; Frechet, J. M. J. *J. Am. Chem. Soc.* **2011**, *133*, 12106−12114.
(49) Wu, Q.; Van Voorhis, T. *Phys. Rev. A* **2005**, *72*, 024502.
(50) Klamt, A.; Schuurmann, G. *J. Chem. Soc., Perkin Trans. 2* **1993**, 799−805.
(51) Vandewal, K.; Gadisa, A.; Oosterbaan, W. D.; Bertho, S.; Banishoeib, F.; Van Severen, I.; Lutsen, L.; Cleij, T. J.; Vanderzande, D.; Manca, J. V. *Adv. Funct. Mater.* **2008**, *18*, 2064−2070.
(52) van Bavel, S.; Sourty, E.; de With, G.; Frolic, K.; Loos, J. *Macromolecules* **2009**, *42*, 7396−7403.
(53) Pauck, T.; Bassler, H.; Grimme, J.; Scherf, U.; Mullen, K. *Chem. Phys.* **1996**, *210*, 219−227.
(54) Valeev, E. F.; Coropceanu, V.; da Silva Filho, D. A.; Salman, S.; Brédas, J.-L. *J. Am. Chem. Soc.* **2006**, *128*, 9882−9886.